Latent Dynamical Variables Produce Signatures of Spatiotemporal Criticality in Large Biological Systems

Mia C. Morrell, Audrey J. Sederberg, and Ilya Nemenman

Latent dynamical variables produce signatures of spatiotemporal criticality in large biological systems

Mia C. Morrell,[1, *] Audrey J. Sederberg,[1, 2] and Ilya Nemenman[1, 3, 2]

[1]*Department of Physics, Emory University, Atlanta, GA 30322, USA*
[2]*Initiative in Theory and Modeling of Living Systems, Emory University, Atlanta, GA 30322, USA*
[3]*Department of Biology, Emory University, Atlanta, GA 30322, USA*
(Dated: January 11, 2021)

Understanding the activity of large populations of neurons is difficult due to the combinatorial complexity of possible cell-cell interactions. To reduce the complexity, coarse-graining had been previously applied to experimental neural recordings, which showed over two decades of apparent scaling in free energy, activity variance, eigenvalue spectra, and correlation time, hinting that the mouse hippocampus operates in a critical regime. We model such data by simulating conditionally independent binary neurons coupled to a small number of long-timescale stochastic fields and then replicating the coarse-graining procedure and analysis. This reproduces the experimentally-observed scalings, suggesting that they do not require fine-tuning of internal parameters, but will arise in any system, biological or not, where activity variables are coupled to latent dynamic stimuli. Parameter sweeps for our model suggest that emergence of scaling requires most of the cells in a population to couple to the latent stimuli, predicting that even the celebrated place cells must also respond to non-place stimuli.

A key problem in modern biological physics is extracting useful knowledge from massive data sets enabled by high-throughput experimentation. For example, now one can record simultaneous states of thousands of neurons [1–5] or gene expressions [6–8], or the abundances of species in microbiomes [9–11]. Inferring and interpreting the joint probability distributions of so many variables is difficult. A promising resolution to the problem is to adapt the Renormalization Group (RG) [12] framework for coarse-graining systems in statistical physics to find relevant features and large-scale behaviors in biological data sets as well. Indeed, RG-inspired coarse-graining showed an emergence of nontrivial scaling behaviors in neural populations [13, 14]. Specifically, the authors analyzed the activity of over 1000 neurons in the mouse hippocampus as the animal repeatedly ran through a virtual maze. Their coarse-graining scheme involved combining the most correlated neurons into neural clusters by analogy with Kadanoff's hyperspins [15], while using cluster-cluster correlations as a proxy for locality. Various correlation functions of neural clusters exhibited self-similarity for different cluster sizes, suggestive of criticality. Further analysis inspired by Wilson's momentum space approach to renormalization [16] revealed that the joint distribution of cluster activities flowed to a non-trivial, non-Gaussian fixed point. The apparent scaling relations persisted for only a decade or two (limited by the size of the experimental system), and it was unclear whether they would exist for larger systems. Nonetheless, the observations were intriguing, and mechanisms responsible for them remain unknown. Thus it is unclear which other systems may exhibit them.

Observation and interpretation of signatures of criticality in high-throughput biological experiments is a storied field [17–22]. As a specific example, one commonly observed signature is the Zipf's law, which describes a power-law relation between the rank and the frequency of a system's states. It has been explained by the existence of stationary latent (unobserved) fields (such as stimuli or internal states) that couple neurons (spins) over long distances [23, 24]. Similarly, here we show that the observations of Ref. [14], including apparent scaling properties of the free energy, the cluster covariance, the cluster autocorrelations, and the flow of the cluster activity distribution to a non-Gaussian fixed point can be explained, within experimental error, by a model of non-interacting neurons coupled to *multiple* latent *dynamical* fields. This *novel* model is the first to explain such a variety of spatio-temporal scaling phenomena observed in large-scale biological data, and to our knowledge, is the first model to explore these phenomena using *multiple time-dependent* latent fields. While developed for the specific neural dataset, the model is much broader: it predicts that similar spatio-temporal scaling relations will emerge without fine-tuning in other multivariate datasets, biological and inanimate, with latent dynamical variables.

Below we introduce the model, implement the coarse-graining of Ref. [14] on data generated from it and compare our findings with experimental results. We conclude by discussing which other experimental systems may exhibit similar apparent scaling relations under the RG procedure.

The model. — To understand how scaling relations could arise from coarse-graining data from large-scale systems, we study a model of N binary neurons (spins) $s_i \in \{0, 1\}, i \in [1, N]$, where $s_i = 0$ or 1 corresponds to a neuron being silent or active. The neurons are conditionally independent and coupled only by N_f fields $h_m(t)$,

---

* Current address: Los Alamos National Laboratory, XCP-8, Los Alamos, NM 87545, USA

$m \in [1, N_{\mathrm{f}}]$ such that the probability of a population being in a certain state $\{s_i\}$ is

$$P(\{s_i\}|\{h_m\}) = \frac{1}{Z(\{h_m\})} e^{H(\{s_i\},\{h_m\})}, \qquad (1)$$

where Z is the normalization, and H is the "energy":

$$H = \eta \left[\sum_{i,m=1}^{N,N_{\mathrm{f}}} h_m(t) W_{im} s_i + \epsilon s_i \right]. \qquad (2)$$

Here ϵ is the bias toward silence, η controls the variance of individual neuron activity, and W_{im} are coupling constants linking neurons to fields. The model includes two types of fields (place and latent), explained below.

In the experiment analyzed in Ref. [14], a mouse ran on a virtual track repeatedly, while neural activity in a population of hippocampal neurons was recorded. A subset of these neurons, called *place cells*, are activated when the mouse is at certain points on the track. To capture this structure, we define place fields distributed along a virtual track of length X. We simulate 200 repetitions of a run along a track of length X with an average forward speed v. As in the experiments, at the end of each run, the mouse is transported instantaneously to the beginning of the track. Thus the mouse position is $x(t) = v(t \mod T)$, where $T = X/v = 1$ is the time to run a track length. The place fields $h_m^{(\mathrm{place})}(x)$ are modeled as Gaussians with centers $\mu_m \sim \mathrm{unif}(0, X]$ and standard deviations $\sigma_m \sim \Gamma(4, X/40)$ drawn from the Γ-distribution with shape 4 and scale $X/40$. Coupling between a spin and its place field $W_{im}^{(\mathrm{place})}$ is nonzero with probability q, with its value drawn from the standard Γ distribution, $\Gamma(1,1)$. We include place fields in our model to match the observed data, but we reproduce the apparent scaling results within error bars whether or not place cells are modeled (see *Discussion* and *Online Supplementary Materials*) [25].

The second type of field is a latent field, which we interpret as processes, such as head position or arousal level, known to modulate neural activity, but not directly controlled or measured by experiment [26]. We model each latent field $h_m^{(\mathrm{latent})}$ as an Ornstein-Uhlenbeck process with zero mean, unit variance, and time constant τ.

TABLE I. Simulation parameters for Figures 1-3.

Parameter	Description	Value
ϕ	latent field multiplier	$\phi = 1.0$
ϵ	bias towards silence	$\epsilon = -2.67$
η	variance multiplier	$\eta = 6.0$
q	probability of coupling to latent field	$q = 1.0$
N_{f}	number of latent fields	$N_{\mathrm{f}} = 10$
τ	latent field time constant	$\tau = 0.1$
$h_m^{(\mathrm{place})}$	presence or absence of place fields	all cells couple to latent fields, half couple to place fields

We model couplings to the latent fields as

$$W_{im}^{(\mathrm{latent})} = \phi \times \begin{cases} \sim \mathcal{N}(0,1) & \text{if } i \text{ couples to latent fields,} \\ 0, & \text{otherwise.} \end{cases} \qquad (3)$$

Here $\sim \mathcal{N}(0,1)$ denotes sampling from the standard normal distribution, and ϕ controls the strength of latent fields relative to place fields. We present results with all latent fields $h_m^{(\mathrm{latent})}$ possessing the same time constant τ (see Tbl. I for parameters), so that temporal criticality cannot be attributed to the diversity of time scales in the fields driving neural activity.

While we explored many different parameter choices (see Tbl. S1), we present results with $N = 1024$ [14], and $N_{\mathrm{f}} = 10$. Consistent with Ref. [14], we choose $p = 50\%$ of neurons to be place cells, each coupled to its own place field (μ_m, σ_m). Each latent field is coupled to every neuron. Thus in our typical simulations, about 512 neurons respond to place and latent stimuli, and about 512 are exclusively latent-stimuli neurons.

Software implementation of the model is available [27].

Results. — In the following, we simulate random neural activity according to Eq. (1) and then replicate the real-space and momentum-space coarse-graining schemes of Ref. [14], while tracking the distributions of variables within clusters as we iterate the coarse-graining algorithms. Briefly, in each iteration of the real-space coarse-graining scheme, pairs of highly correlated neurons are combined into clusters. The cluster activity is the sum of the pair's activity. At each iteration step, the population size is therefore halved. In the momentum-space coarse-graining scheme, neural activity fluctuations are projected onto the eigenvectors of the covariance matrix of the population activity, selecting the K eigenvectors with the largest eigenvalues, and then projected back to the original system size, N. All results of Ref. [14] can be *quantitatively* reproduced by our model, and we include corresponding experimental results in blue on each figure when appropriate. Several scaling exponents were not included or were only reported for a single recording in Ref. [13], and therefore we refer to Ref. [14].

1. Scaling of the activity variance. Real-space coarse-graining of experimental data [14] reported that the variance of the cluster variables scaled with cluster size K as K^α, $\alpha = 1.40 \pm 0.06$, in one experiment. In our simulations, the coarse-grained activity variance scales as K^α, $\alpha = 1.36 \pm 0.01$, over more than two decades in K (Fig. 1A), within error bars of the experimental value. This indicates that the microscopic variables are not fully independent (which would be $\alpha = 1$), nor are they fully correlated (which would be $\alpha = 2$).

2. Scaling of the free energy. The effective free energy is related to the probability of silence in a cluster, and is expected to scale as a power of cluster size, $K^{\tilde\beta}$ [14]. Specifically, we marginalize Eq. (1) over all fields:

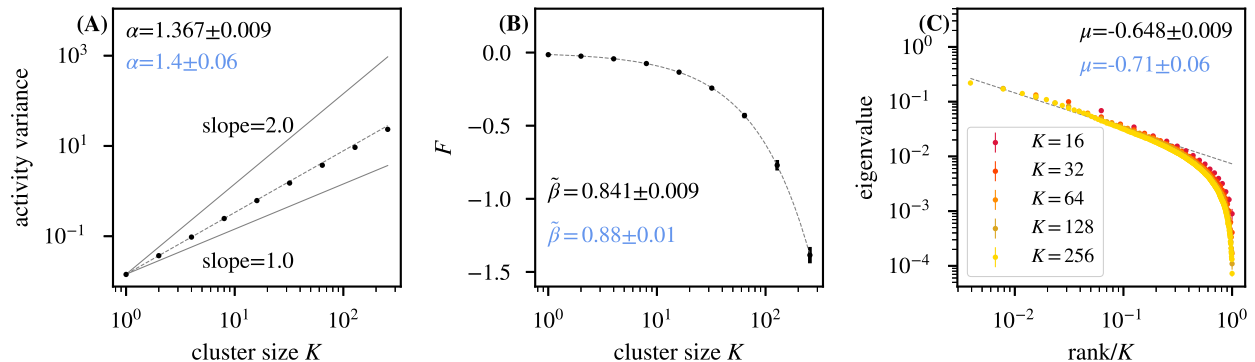$$P(\{s_i\}) = \int d\{h_m\} P(\{h_m\}) P(\{s_i\}|\{h_m\}) \qquad (4)$$

FIG. 1. **(A)** Activity variance of coarse-grained variables at each coarse-graining iteration, fit to $\propto K^{\alpha}$, $\alpha = 1.37 \pm 0.01$. This is within error of the experimental observation $\alpha = 1.4 \pm 0.06$ [14], shown in blue. **(B)** Average free energy, Eq. 5, at each coarse-graining iteration, fit to $\propto K^{\tilde{\beta}}$, $\tilde{\beta} = 0.84 \pm 0.01$, again close to experimentally found $\tilde{\beta} = 0.88 \pm 0.01$ [14]. **(C)** Eigenvalue spectrum of cluster covariance for cluster sizes $K = 32, 64, 128$ against the scaled rank, averaged over clusters. We observe scaling as in Eq. (6) for ~ 1.5 decades with $\mu = 0.65 \pm 0.01$, within error of the experimental $\mu = 0.71 \pm 0.06$ [14]. For all panels, error bars are standard deviations over randomly selected contiguous quarters of the simulation.
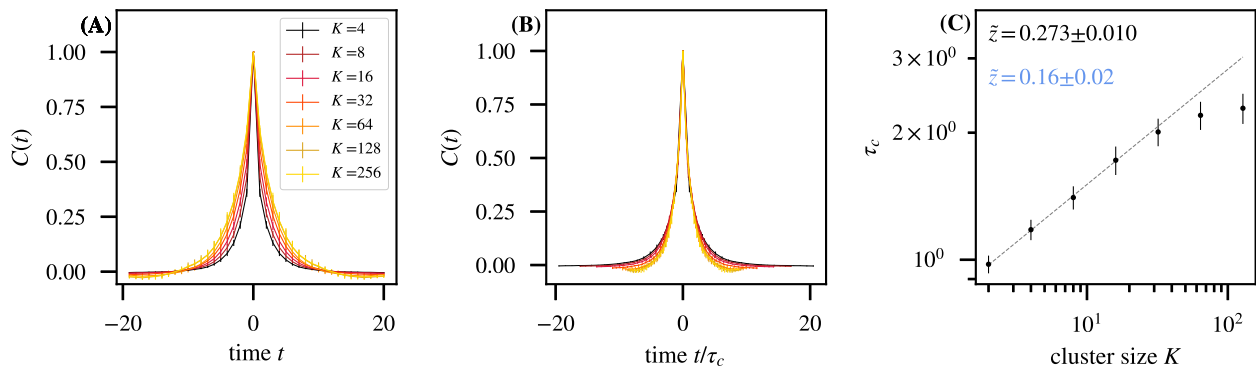

FIG. 2. **(A)** Average autocorrelation function for cluster sizes $K = 2, 4, ..., 256$ as a function of time. **(B)** Same data, but with time rescaled by the appropriate τ_c for each cluster size. **(C)** Time constants τ_c extracted from each curve in **(A)** obey $\tau_c \propto K^{\tilde{z}}$, $\tilde{z} = 0.27 \pm 0.01$, for roughly 1 decade. Experimentally found $\tilde{z}$ is shown in blue [14]. Error bars are standard deviations over randomly selected contiguous quarters of the simulation.

and compute $\ln P(\{s_i = 0\}) = \ln P(\{s_i = 0\}|\{h_m\}) + \ln \sum_{\{h_m\}} P(\{h_m\})$, where $P(\{s_i = 0\})$ is the probability that all neurons $\{s_i\}$ are silent. This defines

$$F(\{s_i\}) = -\ln P(\{s_i = 0\}|\{h_m\}), \qquad (5)$$

where $F(\{s_i\})$ is effective free energy. In Fig. 1B, we observe that the average free energy at each coarse-graining step scales, with exponent $\tilde{\beta} = 0.84 \pm 0.01$, within error bars of experimental results, 0.88 ± 0.01 [14].

3. Scaling of the eigenvalue spectra. We expect the eigenvalues of the covariance matrix of microscopic variables within each cluster to scale as a power law of the scaled eigenvalue rank [14]. Thus there are two scalings: the rank by the cluster size, and the eigenvalue by the scaled rank. Specifically, the Rth eigenvalue λ_R of a clus-

ter of size K was shown in [14] to follow

$$\lambda_R \propto \left(\frac{K}{R}\right)^{\mu}. \qquad (6)$$

In Fig. 1C, we plot the average eigenvalue spectrum of the covariance matrix for each coarse-grained variable for cluster sizes $K = 16, 32, 64, 128, 256$. We observe scaling according to Eq. 6 for roughly 1.5 decades, with scaling exponent $\mu = -0.65 \pm 0.01$, within error bars of the experimental value $\mu = -0.71 \pm 0.06$.

4. Scaling of the correlation time. Another signature of critical systems is that the timescale of cluster autocorrelation τ_c is a power law of length scale (cluster size K) with exponent $\tilde{z}$. In Fig. 2A we plot the average autocorrelation function for $K = 4, 8, ..., 256$. In Fig. 2B, we
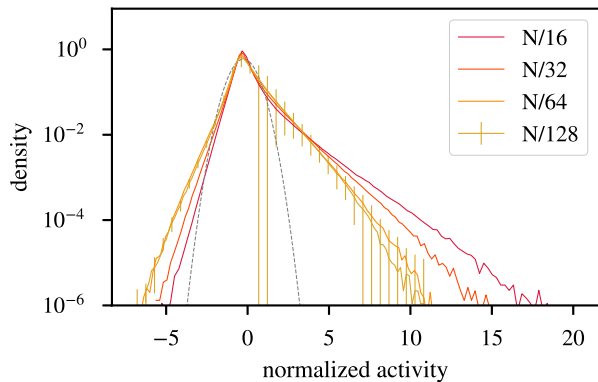
FIG. 3. Distribution of coarse-grained variables for $k = N/16, N/32, N/64, N/128$ modes retained under momentum-space coarse-graining, with a Gaussian distribution (gray dashed line) shown for comparison. Notice that the momentum-space coarse-grained variables may take negative values. The distribution of coarse-grained variables approaches a non-Gaussian limit as k decreases. Error bars are standard deviations over randomly selected contiguous quarters of the simulation.

show the same data as a function of rescaled time, τ/τ_c, where τ_c is calculated by fitting the correlation function to the exponential form. The collapse shown in Fig. 2B suggests that $C(t/\tau_c)$ is scale invariant. We then observe a power law relation between the time constant τ_c and the cluster size K for roughly 1.5 decades in Fig. 2C, with a scaling exponent $\tilde{z} = 0.27 \pm 0.01$. For the recording reported in Ref. [14], the exponent was somewhat different, $\tilde{z} = 0.16 \pm 0.02$, but the value over three different recordings, $\tilde{z} = 0.22 \pm 0.08 \pm 0.10$ (mean, individual recording rms error, standard deviation across recordings) again matches our result.

5. Flow to a non-Gaussian fixed point. We replicated the momentum space coarse-graining analysis of Ref. [14]. We first calculated the covariance matrix Γ_{ij} of the neural activity fluctuations matrix $\Phi_{it} = S_{it} - \langle S_{it} \rangle_t$, where i indexes neurons and t indexes time step. We then calculated the eigenvalues and eigenvectors of Γ_{ij} and constructed a matrix $\tilde{S}_{ij}$ containing the eigenvectors in its columns, ordered by the corresponding eigenvalues, from largest to smallest. Summing over the first k modes, we calculated the coarse-grained variable

$$S_{it}^{(k)} = z_i \sum_{l,j'}^{N,k} \tilde{S}_{ij'} \Phi_{lt} \tilde{S}_{lj'}, \qquad (7)$$

where we set z_i such that $\langle [S_{it}^{(k)}]^2 \rangle_t = 1$ [14].

In Fig. 3, we follow the distribution of $S_{it}^{(k)}$ over coarse-graining cut-offs k. As the coarse-grained variables are linear combinations of the original variables, if correlations between the original variables are weak, the distribution will approach a Gaussian due to the central

limit theorem. However, close to criticality, the system may flow to a non-Gaussian fixed point. We show the distributions of coarse-grained variables $S_{it}^{(k)}$ for $k = N/16, N/32, N/64, N/128$ modes retained, observing the flow to a non-Gaussian limit as k decreases: the limit distribution retains a sharp peak at 0 and a heavy positive tail, similar to experiments [14].

Experimental agreement. To investigate which parameter regimes give rise to scaling in our model, we vary the parameters η, ϕ, and ϵ in Eq. (2), the latent field correlation time τ, the number of latent fields $N_{\rm f}$, and the probability that a neuron couples to a latent field q. We vary them one at a time, while keeping other parameters at values in Tbl. I. We also run simulations with only latent fields $h_m^{(\text{latent})}$, or with only place fields $h_m^{(\text{place})}$. We record parameters whose simulations display eigenvalue spectra collapse for at least 1.5 decades, as in Fig. 1D, and activity variance scaling for over 2 decades, as in Fig. 1A. Parameter regimes leading to apparent scaling are summarized in Tbl. S1, with detailed plots shown in *Online Supplementary Materials* [25]. We show scatter plots of pairs of scaling exponents (if scaling is observed) in Fig. S8, compared to the values from three different experiments as reported in Ref. [14]. Our simulations show that a broad range of parameters lead to scaling exponents in quantitative agreement with experiments. Briefly, to achieve nontrivial robust scaling, one crucially needs ≥ 5 strong latent fields, as well as a strong bias towards silence.

Discussion. — When the number of activity variables is large, working with their joint probability distributions is hard, and one coarse-grains to develop interpretable models of the data. We have shown that, under two different coarse-graining schemes, a model of population activity, in which neurons (spins) are randomly coupled to a few slowly varying latent stimuli or fields (certainly an amount insufficient to overfit the data) replicates power law scaling relationships *and* the flow of activity distributions to a non-Gaussian fixed point, reported in mouse hippocampus experiments [13, 14]. Other models, such as a randomly connected rate network [28], or a spiking Brunel neural network in the synchronous irregular regime [29], cannot reproduce these results [14]. In the latter case, one can approximate the network by a population of uncoupled neurons driven by a single common time-varying input [20], but we show that the emergence of scaling requires *multiple time-dependent* latent processes, explaining why previous models cannot reproduce these hippocampal data.

Our parameter sweeps show that emergence of scaling in the model is robust to parameter changes. The existence of scaling is most sensitive to nearly all cells having significant latent field coupling, irrespective of whether they additionally couple to place fields. This is especially clear in Fig. S13, where only simulations with widespread latent field coupling reproduce the autocorrelation time collapse [25]. This allows us to make an interesting – and testable – biological prediction that even place cells in

hippocampus must be driven not solely by the animal's position. This is consistent with the observations that place cells carry about as much information about activity of other cells in the population as they carry about the animal's position [30]. Further, since it is difficult to reproduce temporal scaling over many decades using latent fields with a single time constant, but diversity of time constants makes it easier (see *Online Supplementary Materials*) [25]), another testable prediction of our analysis is that the latent fields are likely to have diverse time scales.

More broadly, we have shown that the surprising spatio-temporal scaling results of Ref. [14] can be explained by the presence of multiple unknown, time-varying latent fields (possibly with just a single time constant). To our knowledge, this is the first model able to explain such observations, though models of related spatio-temporal scaling phenomena (e. g., neural avalanches) certainly exist [31]. The coarse-graining approach we study here, and especially the momentum space analysis, has been shown effective in distinguishing critical and non-critical models [32]. This makes it even more surprising that the approximately scale-free distributions *necessarily* emerge under renormalization in our

class of models, which do not require fine-tuning, and that the scaling relations become more robust for larger systems sizes (see *Online Supplementary Materials*) for results with an order of magnitude more neurons [25]). This raises questions whether and when apparent scaling in multivariate biological systems can be viewed as evidence of more traditional criticality, which emerges through fine-tuning of internal interaction parameters. While here we have focused on neural data, our more important result is the prediction that the apparent scaling relations discussed in this *Letter*, whether they should be viewed as signatures of criticality or not, will emerge from *any* sparsely active multivariate system (whether biological, inanimate, social, or human-made) driven by several latent dynamical processes.

ACKNOWLEDGMENTS

[1] R. Segev, J. Goodhouse, J. Puchalla, and M. J. Berry, Nature Neuroscience **7**, 1155 (2014).

[2] J. Nguyen, F. Shipley, A. Linder, G. Plummer, J. Shaevitz, A. Leifer, and S. Setru, Proceedings of the National Academy of Sciences **113** (2015).

[3] J. L. Gauthier and D. W. Tank, Neuron **99**, 179 (2018).

[4] D. A. Schwarz, M. A. Lebedev, T. L. Hanson, D. F. Dimitrov, G. Lehew, J. Meloy, S. Rajangam, V. A. Subramanian, P. J. Ifft, Z. S. Li, A. Ramakrishnan, A. J. Tate, K. Z. Zhuang, and M. A. L. Nicolelis, Nature methods **11**, 670 (2014).

[5] Q. Lin, J. Manley, M. Helmreich, F. Schlumm, J. M. Li, D. N. Robson, F. Engert, A. Schier, T. Nbauer, and A. Vaziri, Cell **180**, 536 (2020).

[6] G. X. Y. Zheng, J. M. Terry, P. Belgrader, P. Ryvkin, Z. W. Bent, R. Wilson, S. B. Ziraldo, T. D. Wheeler, G. P. McDermott, J. Zhu, M. T. Gregory, J. Shuga, L. Montesclaros, J. G. Underwood, D. A. Masquelier, S. Y. Nishimura, M. Schnall-Levin, P. W. Wyatt, C. M. Hindson, R. Bharadwaj, A. Wong, K. D. Ness, L. W. Beppu, H. J. Deeg, C. McFarland, K. R. Loeb, W. J. Valente, N. G. Ericson, E. A. Stevens, J. P. Radich, T. S. Mikkelsen, B. J. Hindson, and J. H. Bielas, Nature communications **8**, 14049 (2017).

[7] J. Cao, J. S. Packer, V. Ramani, D. A. Cusanovich, C. Huynh, R. Daza, X. Qiu, C. Lee, S. N. Furlan, F. J. Steemers, A. Adey, R. H. Waterston, C. Trapnell, and J. Shendure, Science **357**, 661 (2017).

[8] T. M. Gierahn, M. H. Wadsworth, T. K. Hughes, B. D. Bryson, A. Butler, R. Satija, S. Fortune, J. C. Love, and A. K. Shalek, Nature methods **14**, 395398 (2017).

[9] H. G. Martn and N. Goldenfeld, Environmental Microbi-

ology **8**, 1145 (2006).

[10] C. Palmer, E. M. Bik, D. B. DiGiulio, D. A. Relman, and P. O. Brown, PLOS Biology **5**, 1 (2007).

[11] N. M. Vega and J. Gore, PLOS Biology **15**, 1 (2017).

[12] N. Goldenfeld, *Lectures on Phase Transitions and the Renormalization Group* (2018) pp. 1–394.

[13] L. Meshulam, J. L. Gauthier, C. D. Brody, D. W. Tank, and W. Bialek, Phys. Rev. Lett. **123**, 178103 (2019).

[14] L. Meshulam, J. L. Gauthier, C. D. Brody, D. W. Tank, and W. Bialek, Coarse–graining and hints of scaling in a population of 1000+ neurons, arXiv:1812.11904. (2018).

[15] L. P. Kadanoff, Physics Physique Fizika **2**, 263 (1966).

[16] K. G. Wilson, Rev. Mod. Phys. **55**, 583 (1983).

[17] T. Mora, A. M. Walczak, W. Bialek, and C. G. Callan, Proceedings of the National Academy of Sciences **107**, 5405 (2010).

[18] J. E. S. Socolar and S. A. Kauffman, Phys. Rev. Lett. **90**, 068702 (2003).

[19] M. Nykter, N. D. Price, M. Aldana, S. A. Ramsey, S. A. Kauffman, L. E. Hood, O. Yli-Harja, and I. Shmulevich, Proceedings of the National Academy of Sciences **105**, 1897 (2008), https://www.pnas.org/content/105/6/1897.full.pdf.

[20] J. Touboul and A. Destexhe, Physical Review E **95**, 1 (2017), arXiv:1503.08033.

[21] J. P. Barton, M. Kardar, and A. K. Chakraborty, Proceedings of the National Academy of Sciences of the United States of America **112**, 1965 (2015).

[22] D. R. Chialvo, Nature Physics **6**, 744 (2010).

[23] L. Aitchison, N. Corradi, and P. E. Latham, PLOS Computational Biology **12**, 1 (2016).

[24] D. J. Schwab, I. Nemenman, and P. Mehta, Phys. Rev.

Lett. **113**, 068102 (2014).

[25] See Supplemental Material at [URL will be inserted by publisher] for details concerning pairwise correlations, place cell activity, and parameters sweeps in our simulations.

[26] M. J. McGinley, M. Vinck, J. Reimer, R. Batista-Brito, E. Zagha, C. R. Cadwell, A. S. Tolias, J. A. Cardin, and D. A. McCormick, Neuron **87**, 1143 (2015).

[27] M. Morrell, A. Sederberg, and I. Nemenman, placerg – A Python package for simulation and coarse-graining analysis of time-dependent latent variable models.

[28] C. V. Vreeswijk and H. Sompolinsky, Science **274**, 1724 (1996).

[29] N. Brunel, Journal of Computational Neuroscience **8**, 183 (2000).

[30] L. Meshulam, J. L. Gauthier, C. D. Brody, D. W. Tank, and W. Bialek, Neuron **96**, 1178 (2017).

[31] T. Mora, S. Deny, and O. Marre, Phys. Rev. Lett. **114**, 078105 (2015).

[32] G. Nicoletti, S. Suweis, and A. Maritan, Phys. Rev. Research **2**, 023144 (2020).